Effects of Aerosol Size and Coating Thickness on the Molecular Detection using Extractive Electrospray Ionization

Chuan Ping Lee,[1] Mihnea Surdu,[1] David M. Bell,[1] Houssni Lamkaddam,[1] Mingyi Wang,[2,3] Farnoush Ataei,[6] Victoria Hofbauer,[2,3] Brandon Lopez,[2,4] Neil M. Donahue,[2,3,4,5] Josef Dommen,[1] Andre S. H. Prevot,[1] Jay G. Slowik,[1] Dongyu Wang,[1,] Urs Baltensperger,[1] Imad El Haddad[1,*]*

[1]Laboratory of Atmospheric Chemistry, Paul Scherrer Institute (PSI), 5232 Villigen, Switzerland.
[2]Center for Atmospheric Particle Studies, Carnegie Mellon University, Pittsburgh, PA, 15213, USA.
[3]Department of Chemistry, Carnegie Mellon University, Pittsburgh, PA, 15213, USA.
[4]Department of Chemical Engineering, Carnegie Mellon University, Pittsburgh, PA, 15213, USA.
[5]Department of Engineering and Public Policy, Carnegie Mellon University, Pittsburgh, PA, 15213, USA
[6]Leibniz-Institute for Tropospheric Research, 04318 Leipzig, Germany.

Correspondence to: Imad El Haddad (imad.el-haddad@psi.ch), Dongyu Wang (dongyu.wang@psi.ch), Jay G. Slowik (jay.slowik@psi.ch)

Abstract. Extractive electrospray ionization (EESI) is a well-known technique for high throughput online molecular characterization of chemical reaction products and intermediates, detection of native biomolecules, in vivo metabolomics, and environmental monitoring with negligible thermal and ionization-induced fragmentation for over two decades. However, the EESI extraction mechanism remains uncertain. Prior studies disagree whether particles between 20 and 400 nm diameter are fully extracted or if the extraction is limited to the surface layer. Here, we examined the analyte extraction mechanism by assessing the influence of particles size and coating thickness on the detection of the molecules therein. We find that particles are extracted fully: Organics-coated NH_4NO_3 particles with a fixed core volume (156 and 226 nm in diameter without coating) show constant signals for NH_4NO_3 independent of the shell coating thickness, while the signals of the secondary organic molecules comprising the shell varied proportionally to the shell volume. We also find that the EESI sensitivity exhibits a strong size dependence, with an increase in sensitivity by one to three orders of magnitude as particles size decreases from 300 nm to 30 nm. This dependence varies with the electrospray (ES) droplet size, the particles size and residence time for coagulation in the EESI inlet, suggesting that the EESI sensitivity is influenced by the coagulation coefficient between particles and ES droplets. Overall, our results indicate that, in the EESI, particles are fully extracted by the ES droplets regardless of the chemical composition, when they are collected by the ES droplets. However, their coalescence is not complete and depends strongly on their size. This size-dependence is especially relevant when EESI is used to probe size-varying particles as is the case in aerosol formation and growth studies with size ranges below 100 nm. In contrast, it does not significantly influence the detection of ambient aerosol dominated by particle sizes ranging between 100 - 2500 nm, i.e. the accumulation mode.

1 Introduction

Atmospheric aerosols are suspended particles in the air ranging from a few nanometers (nm) to several micrometers (μm) in diameter. Fine particles (< 1 μm) comprise nucleation, Aitken and accumulation mode particles, and account for 50-70 % of the total particulate matter (PM) mass concentrations in polluted environments (Yue et al., 2009). They can affect the earth's radiative balance either directly, by interacting with solar radiation, or indirectly by acting as cloud condensation nuclei (CCN), influencing cloud albedo and lifetime (Steinfeld, 1998). Exposure to PM is one of the leading causes for premature death, accounting for ~8.9 million deaths, or ~10% of total global burden of mortality in 2015 (Burnett et al., 2018), though the underlying mechanisms remain uncertain (Daellenbach et al., 2020). PM can be emitted as primary aerosol or produced in the atmosphere after chemical reactions via nucleation or condensation of gas-phase products (Berndt et al., 2005; Clarke et al.,

1984; Hoffmann et al., 1997; Jimenez et al., 2009; Kalberer et al., 2004; Kirkby et al., 2011). Heterogeneous reactions may also further increase the complexity of ambient aerosol mixtures (George and Abbatt 2010; Ditto et al., 2020).

Online molecular characterization of atmospheric aerosols is required to resolve the spatiotemporal variability of PM molecular composition and to identify PM sources. Progress has been made with the development of chemical ionization interfaces such as the Filter Inlet for Gases and AEROsols (FIGAERO) (Lopez-Hilfiker et al., 2014), Thermal Desorption Differential Mobility Analyzer (TD-DMA) (Holzinger et al., 2010; Wagner et al., 2018), and Chemical Analysis of Aerosol Online (CHARON) (Eichler et al., 2015) coupled to a mass spectrometer. However, these techniques suffer from thermal decomposition of the analyte prior to ionization and/or ionization-induced fragmentation, impeding molecular speciation (Müller et al., 2017; Stark et al., 2017). To complement these instruments, an extractive electrospray (ES) ionization time-of-flight mass spectrometer (EESI-TOF) was developed to enable molecular characterization of organic aerosol at 1 Hz time resolution with ng m^{-3} level detection limit, and minimal thermal and ionization-induced fragmentation (Lopez-Hilfiker et al., 2019). The EESI-TOF was further developed to enable online tandem mass spectrometry for molecular structure elucidation, and to characterize water-soluble metals (Giannoukos et al., 2020; Lee et al., 2020).

Several studies such as extraction of macromolecules from colloidal solution (Chen et al., 2006), electron-transfer-catalyzed dimerization (Marquez et al., 2008), and gas plume mixing in the charged droplets (Cheng et al., 2008), reported that the ionization of EESI mainly happens in the liquid phase via interaction between ES charged droplets and neutral analyte droplets. For clarity, we refer to our neutral analyte droplets as "particles" prior to their interaction with ES droplets and as "analyte-laden droplets" afterwards. If this liquid-phase extraction of EESI occurs via total coalescence between particles and ES droplets, the measured EESI signal should be proportional to the total analyte mass concentration, i.e. full extraction of particles by ES droplets as demonstrated by several studies (Law et al., 2010; Lopez-Hilfiker et al., 2019). In contrast, new studies suggested that the particles are only partially probed, limiting the full quantification of the extracted analyte with electrospray ionization (Wang et al., 2012, Kumbhani et al., 2018). Kumbhani et al. (2018) suggested that only the surface of particles with a diameter size of approximately 100 nm is extracted by comparing infusion ESI-MS with EESI-MS using coated chemical standards (Kumbhani et al., 2018). Using other techniques such as phase Doppler anemometer, Wang et al. (2012) suggested that the extraction happens via fragmentation of the analyte droplets and ES droplets as the result of droplet-droplet collisions (Wang et al., 2012). Finally, other studies have proposed that the EESI extraction efficiency could depend on the analyte volatility and size (Meier et al., 2011a; Pagonis et al., 2020). Since all these studies only probed simple systems i.e. individual chemical standards using one kind of experimental and EESI ionization source, these discrepancies could be inherently attributed to their differences of ES ionization geometries, experimental conditions, irreproducible ES Taylor cone conditions and perhaps the choices of chemicals.

Nevertheless, without reconciling the discrepancies of these reported EESI mechanisms, EESI quantification must be regarded as highly uncertain when the technique is used to probe varying size distributions of particles that exist in different mixing states and are comprised of different molecular polarity, volatility, and sizes. Here, we take advantage of recent advancements in particle generation and chemical analysis to evaluate the extraction mechanism of EESI using three different methods for particles generation and several online mass spectrometers for aerosol online chemical analysis. First, we characterize the EESI extraction efficiency with particles containing atmospherically relevant standard compounds and mixtures, selected in the size range 30-500 nm using an aerosol aerodynamic classifier. We elucidate the influence of the ES operating parameters and residence time between ES droplets and particles using two different EESI sources. Second, we assess whether the EESI extraction efficiency depends on the analyte chemical composition, by comparing EESI-TOF and a chemical ionization (CI) TOF-MS equipped with a Filter Inlet for Gases and AEROsols (FIGAERO) sampling manifold (FIGAERO-CI-ToF-MS) measurements for α-pinene secondary organic aerosol (SOA) generated in the CLOUD (Cosmics Leaving OUtdoor Droplets) chamber at CERN, Switzerland (Kirkby et al., 2016; Tröstl et al., 2016; Dias et al., 2017). Third, we determine whether

particles are fully extracted or if extraction is limited to the coated surface by coating monodisperse NH_4NO_3 particles at a fixed size with variable amounts of oxidation products in an oxidation flow tube reactor.

2 Experimental

2.1 Materials

Acetonitrile (Sigma-Aldrich, UV grade), sodium iodide (Sigma-Aldrich, 99.7% purity) and milli-Q water (18 MΩ cm) were used to prepare the electrospray (ES) and chemical standard nebulization solution. Polyimide-coated fused silica capillary (inner diameter (i.d.): 75 µm, outer diameter (o.d.): 369 µm; BGB Analytik, Boeckten, Switzerland), HEPA capsule filter (Pall Corporation), PEEK tubing (i.d.: 500 µm, o.d.: 1/16 inch; BGB Analytik, Boeckten, Switzerland) and charcoal denuders (Ionicon GmbH, Austria) were used for the electrospray ionization inlet. As chemicals, α-Pinene (Sigma-Aldrich, 99% purity), levoglucosan (Sigma-Aldrich, 99% purity), sucrose (Sigma-Aldrich, 99% purity), ammonium nitrate (Sigma-Aldrich, 98% purity) were used.

2.2 Electrospray ionization configuration

Two designs of the EESI sources with a factor of 2 difference in their residence time in the electrospray ionization region were used in this experiment, coupled in front of a high-resolution TOF mass spectrometer (HTOF, Tofwerk AG, Switzerland). EESI source A (Lopez-Hilfiker et al., 2019) and B were developed initially for Tofwerk TOF and Thermo Scientific Orbitrap mass analyzers (Figure S1), respectively, though EESI source B is compatible for both mass analyzers, as described in detail elsewhere (Lee et al., 2020). Source A was used throughout the whole experiment and Source B was only used in the study of Figure 2. Two electrospray (ES) solutions were used to generate charged ES droplets: (1) acetonitrile/H_2O (50/50 v/v); and (2) 100% H_2O (Table S1). Both solutions were doped with 100 ppm NaI. A potential difference of around 2.6-2.9 kV relative to the MS interface was applied to the ES solution, and an air pressure difference of 120 to 800 mbar was applied to the ES solution bottle reservoir, delivering 0.3 - 23 µl min^{-1} of ES solution via a polyimide fused silica capillary (o.d.: 369 µm and i.d.: 50, 75 and 100 µm, BGB Analytik, Switzerland). Different ES operating parameters with estimated ES parent droplet size ranging from 0.7 – 5.66 um are tabulated in Table S2. The ES droplets intersected with the particles before entering the heated TOF-capillary kept at 275 °C (<1 ms residence time), undergoing a Coulomb explosion as the ES droplets evaporated. The generated ions from organic molecules were detected predominantly (> 95 % relative abundance) as sodiated adducts ($[M+Na]^+$) in the positive ionization mode by the HTOF. Ammonium nitrate (NH_4NO_3), an inorganic salt, was detected as $[NaNO_3+Na]^+$. The raw mass spectra (1 Hz) were post-averaged every 10 seconds using Tofware (version 2.5.13). All measured analyte signals were normalized by the most abundant electrospray ion (i.e. $[NaI+Na]^+$) to account for the variation of the electrospray signal (± 5 %).

2.3 Particle size selection

Figures S2 and S3 show two experimental setups for the investigation of the size-dependence of the particles extraction efficiency using EESI. Chemical standards were used in the first experimental setup (Figure S2). Three individual aqueous solutions containing 4000 ppm of levoglucosan, sucrose and ammonium nitrate, respectively, were nebulized separately at 1.4 L min^{-1}, which was then mixed with a 1.6 L min^{-1} make-up zero air. The output particles were dried with a custom-made drier containing silica gel (< 5 % RH) and subsequently size selected using an aerosol aerodynamic classifier (AAC; Cambustion, United Kingdom) to produce monodisperse particles (Tavakoli and Olfert 2013, 2014; Tavakoli et al., 2014). The size selection was implemented by centrifugal separation of the particles according to their mass. Unlike size selection using differential mobility analyzers (Lopez-Hilfiker et al., 2019), size selection using the AAC does not require electrical charging, thereby avoiding multi-charging artifacts. The possible multi-charging of particles might affect the normal extraction condition by the

EESI where the particles are assumed to be neutral (Kebarle and Verkcerk 2009, 2012). In addition, doubly charged particles could result in underestimation of particles size and mass concentration. Therefore, the new experimental setup we propose here is well suited for the study of the EESI size-dependence sensitivity.

After particles size selection, the sample was drawn through a multichannel charcoal denuder to strip gas-phase constituents before entering the EESI-TOF inlet manifold. The sample was also characterized immediately upstream of the electrospray region by a nano-scanning mobility particle sizer (size range 2.5 - 239 nm, nano-SMPS, TSI Inc., USA), a scanning mobility particle sizer (size range 16 - 638 nm, TSI SMPS, TSI Inc., USA) and an aerosol mass spectrometer equipped with a long time-of-flight mass analyzer (AMS-LTOF, Aerodyne Research Inc., USA) (Figure S2). The high concentration of the chemical solutions ensured that sufficiently high analyte concentrations (> 3 μg m^{-3}) remain after size-selection by the AAC using the highest possible sheath flow (15 L min^{-1} at an aerodynamic diameter D_{ae} > 150 nm) to produce highly monodisperse particles distributions (Tavakoli and Olfert 2014) at 30 - 40 % RH. A HEPA filter was used for the background measurements after each particles size-selection.

In the second configuration (Figure S3), we investigated the size-dependent sensitivity of the EESI using biogenic SOA produced from α-pinene oxidation in the Cosmic Leaving OUtdoor Droplets (CLOUD) chamber at CERN, Switzerland (Kirkby et al., 2011, Dias et al., 2017), at -50 to -30 °C and 20 - 60 % RH (Simon et al., 2020). The EESI-TOF signals of individual α-pinene oxidation products ($C_{10}H_{16}O_{3\text{-}8}$) were compared to FIGAERO-CI-ToF-MS (Lopez-Hilfiker et al., 2014). The FIGAERO-CI-ToF-MS measured both the gas and particle phase. Here, particles were first collected onto a 24-mm diameter PTFE filter via a dedicated port with a sampling flow rate of 6 L min^{-1}. Then, 2.7 L min^{-1} of pure N_2 was heated progressively to thermally desorb and vaporize the collected particles during each 14-minute desorption cycle, with the filter temperature varying from 20 to 150 °C at a rate of 10 °C min^{-1}. The desorbed vapor analytes were sampled into a 150 mbar ion-molecule reactor and chemically ionized by iodide (I^-) ions generated by passing a gas stream containing CH_3I through a ^{210}Polonium radioactive source before entering an LTOF mass analyzer for separation. The signal of the FIGAERO-CI-ToF-MS was integrated over the period of particle desorption. The organic analytes were detected predominantly in the form of iodide adducts $[M+I]^-$ (> 95% relative abundance). The sample collection efficiency of the filter used by the FIGAERO-CI-ToF-MS is expected to be higher than 99.9 % for particles above 10 nm (Hilfiker-Lopez et al., 2014). The volume-weighted geometric mean diameters were determined using an SMPS (size range 9 - 834 nm, Leibniz Institute for Tropospheric Research, Germany). The SMPS(s) used for the measurements of chemical standards and α-pinene SOA were calibrated using size standards of polystyrene latex beads.

2.4 Particle surface coating

A 104 cm long Pyrex flow tube of 7.4 cm inner diameter with a total volume of approximately 5 L was used for particle surface coating experiments (Figure S4) (Molteni et al., 2018). A 1000 ppm NH_4NO_3 solution in pure water was nebulized at 1.4 L min^{-1} and dried before size-selection by the AAC (< 5% RH). The resulting NH_4NO_3 particles passed through the charcoal denuders before entering concentrically into the flow tube with a laminar zero air sheath flow of 10 L min^{-1} at 20 °C and 60% RH. Measurements were performed downstream of the flow tube. Particle composition and size were measured by the EESI-TOF and SMPS (16 - 615 nm), respectively. Two different core sizes (155.8 and 226.4 nm) of NH_4NO_3 particles were used for the coating experiments. 4.7 ± 0.4 ppm α-pinene, as measured by a quadrupole proton-transfer-reaction mass spectrometer (Q-PTR), was injected into the reactor from a glass vial with a zero air carrier flow (1 L min^{-1}). To generate ozone, 20 - 200 mL min^{-1} zero air (60% RH at 20 °C) was irradiated by an amalgam lamp (185 and 254 nm; WISAG GmbH, Switzerland). Ozone was mixed with α-pinene to produce ozonolysis products which condensed onto, i.e. "coated" the NH_4NO_3 particles inside the flow tube. Note that depending on the conditions this coating may either result in a core-shell structure or in formation of a homogeneous single phase, though the exact morphology does not affect the conclusion regarding surface extraction, as discussed below. The coating period in the flow tube was approximately 26 ± 0.5 s. The coating thickness was

controlled by varying the ozone concentration in the presence of excess α-pinene, which was measured by a Thermo 49A ozone analyzer (Thermo Fisher Scientific, US) to be 20 - 310 ppb. This ozone concentration range was optimized before injecting the NH_4NO_3 particles to ensure that no nucleation occurred which would have resulted in particles consisting only of SOA. At the beginning of each ozone concentration step, the EESI-TOF sampled the gas and aerosol mixture through a bypass channel without denuder to ensure that all oxidation product signals reached steady state (< 20 min). Afterwards, routine sampling alternated between filtered background (5 min) and particle-phase measurements (10 min). This coating experiment was carefully designed to achieve high condensational growth rates of about 0.8 nm s^{-1} with negligible nucleation.

3 Results and discussion

3.1 Influence of particles size on EESI-TOF detection

Figure 1a shows a typical measurement of the EESI-TOF and SMPS for size-selected sucrose particles. Two sheath flow rates (5 and 15 with L min^{-1}) at 1.4 L min^{-1} of particle flow were used to generate two different full width at half maximum size distributions for demonstrating the precision adjustment of AAC in size-selection. Due to the factor of 3 increase of the AAC sheath flow, the geometric standard deviation σ_g of the size-selected sucrose particle distribution decreased from 1.4 to 1.2. A comparison of the signals in the red windows in Figure 1b shows that the sucrose signal did not increase commensurately with the mass concentration measured by the SMPS (regardless of σ_g), as the volumetric geometric mean diameter of the particles increased. To quantify this effect, we first define the size-dependent sensitivity $S(D_P)$ as

$$S(D_P) = \frac{I(D_P)}{M(D_P)}, \quad (1)$$

where $I(D_P)$ is the intensity of the analyte (Figure 2) or the total intensity of fitted organic ions (Figure 3a) that is normalized by the most abundant electrospray ion ($NaINa^+$) to account for the ES fluctuation (< 5%), the $M(D_p)$ is the mass concentration of the particles measured by the SMPS or/and the AMS-LTOF as a function of the volumetric geometric mean mobility diameter D_P. To show the relative change of the sensitivity as a function of D_P, this sensitivity is normalized by the sensitivity at 100 nm electrical mobility diameter, defined as normalized sensitivity, $S_{100\ nm}$

$$S_{100\ nm} = \frac{S(D_P)}{S(D_P=100\ nm)}, \quad (2)$$

where $S(D_P = 100\ nm)$ was interpolated with respect to a 3 parameters-fitting using the model function $S(D_P, P_1, P_2, P_3) = P_1 \cdot Dp\hat{}(P_2) + P_3$. The normalization by the sensitivity at 100 nm is chosen to accommodate and compare all datasets in this study.

We investigated the normalized sensitivities of the EESI-TOF for levoglucosan, sucrose and NH_4NO_3 (tracers of biomass and anthropogenic activities in the ambient atmosphere) using different EESI ionization sources and ES operating parameters that resulted in different ES parent droplet diameters as estimated in Tables S1, S2 and S3. Figure 2 shows the normalized sensitivity of the size-selected particles at 100 nm (Eq. 2), as a function of the volumetric geometric mean diameter of the particles generated using both pure component and mixed solutions detected under different ES conditions (see also Figure S6, Tables S1-S3). The $S_{100\ nm}$ for different types of particles decreases by up to 3 orders of magnitude as the volumetric geometric mean diameter increases from 30 to 300 nm, and some of them start to reach a plateau at larger sizes for experiments using EESI source A and B. The size-dependent sensitivity is observed for both single compounds and compound mixtures (Figure S6), indicating that the size-dependent sensitivity of the particles is independent of their mixing state of different chemicals.

If we assume that the detected ions from the size-selected particles in EESI are generated after coagulation and extraction between the particles and ES droplets, the normalized sensitivity $S_{100\ nm}$ is interpreted as the total coagulated mass. The determination of the total coagulated mass requires Brownian coagulation coefficients (*BCC*, computed from the particle and

ES droplet sizes), number concentrations and residence time. However, the actual ES droplet size distribution could not be measured using other physical processes because these additional processes could alter the ES droplets properties and affect the electrospray ionization. Therefore, we could only calculate the *BCC* for different size-selected monodisperse particles assuming ES parent droplet sizes of 0.5, 1.5 or 5 μm. These three chosen ES parent droplet sizes represent the likely range of the actual ES droplet sizes, which is theoretically estimated from our ES operating parameters as summarized in Table S2, based on SI Eq. 3-6 and Figure S7. The calculated *BCC* values were normalized to the *BCC* for 100 nm monodisperse particles, denoted as $BCC_{100\ nm}$, as shown in Figure S6a, analogous to the normalization for $S_{100\ nm}$. Most normalized sensitivities (i.e. normalized total coagulated masses) correlate well with the $BCC_{100\ nm}$, as shown in Figure 2. Smaller particle sizes that have higher BCC are collected more efficiently and thus contribute a higher percentage of their total mass for extraction. Furthermore, the plateaus of $S_{100\ nm}$ at larger particles sizes could be explained by the suggested behavior of $BCC_{100\ nm}$ when the size of the particle is similar to the actual ES droplet size or partly to the estimated ES parent droplet size in our study. The high deviation of size-dependent sensitivity (~50 %) for D_p > 200 nm is likely due to the variation of the actual ES droplet size distribution in different calibration runs, which can deviate from the estimated ES parent droplet size. Knowledge of the actual ES droplet size distribution is needed to further explain the variabilities but are beyond the scope of the current study.

It is intuitive that the total coagulated mass for extraction is also dependent on the residence time for coagulation between the particles and the ES droplets during electrospray ionization. Longer residence time would allow for higher fractions of particles to be extracted, i.e. the coagulation of smaller particles would saturate, while the coagulation of larger particles would continue, which would result in a smaller range of size-dependent total coagulated mass, i.e. shallower sensitivity size dependence. We examined this hypothesis by using an EESI source B which provides a factor of 2 longer residence time in the electrospray ionization region. As shown in Figure 2, the sensitivity size dependence resulting from EESI source B (yellow markers), which has twice the residence time as EESI source A, is significantly shallower than the one from EESI source A (blue markers), consistent with our hypothesis. Overall, Figure 2 suggests that the size-dependent sensitivity (total coagulated mass) is dependent on the Brownian coagulation coefficient, which varies with the ES droplet size attributed to the ES operating parameters, as well as the residence time for coagulation. Such size dependence suggests that the ionization of analyte particles in the EESI proceeds through coagulation at a certain size-dependent efficiency, e.g. partial coalescence between particles and ES droplets, as reported by the previous studies (Wang et al., 2012; Kumbhani et al., 2018; Pagonis et al., 2020).

Konermann et al. (2013) reported that the electrospray droplet evaporation can be affected by the size and the polarity of analyte molecules, while Meier et al. (2011) suggested that the extraction efficiency of EESI can depend on the volatility of analyte molecules. We investigated the EESI size dependence sensitivity for a complex mixture of internally mixed α-pinene oxidation products formed in the CLOUD chamber, to evaluate whether such dependence varies with the compounds' volatility, e.g. if volatile species preferentially evaporate from smaller particles before their subsequent ionization. We generated unimodal size distributions of secondary organic aerosol (SOA) with volumetric geometric mean diameters ranging from 17 to 137 nm (Figure S8 and Figure S9). Figure 3a shows the normalized sensitivity of the sum of the detected organic ions measured by EESI-TOF after high-resolution peak fitting, S_{100nm}, as a function of the measured particle size. S_{100nm} decreases from a value of 6 at D_p = 17 nm to ~1 at D_p = 110 nm. The relative change in normalized sensitivity is similar to the results obtained for individual chemical standards presented in Figure 2 for EESI source A. To examine whether there is a composition dependence on the EESI extraction, we compared the signals for the $C_{10}H_{16}O_{3\text{-}8}$ compounds measured by the EESI-TOF and the FIGAERO-CI-ToF-MS as shown in Figure 3b (see also Figure S10) from SOA formation at different temperatures in the CLOUD chamber.

The linear behaviours from different measured species between the EESI-TOF and the FIGAERO-CI-TOF-MS show that the relative abundances of the sampled aerosol chemical composition are similar and comparable for both instruments with negligible re-volatilization of particles at two different sampling points. Thermal decomposition may affect the absolute quantification of particle-phase compounds by the FIGAERO-CI-ToF-MS (Stark et al., 2017). However, to the best of our

knowledge, no size dependence has been reported in the literature for this thermal artefact, which should be cancelled after sensitivity normalization comparison in relative scale for each species of FIGAERO-CI-ToF-MS. The sensitivity size dependence appears to be similar for $C_{10}H_{16}O_{3-8}$ compounds with estimated saturation vapor concentrations ranging from 10^{-10} to 10^{4} μg m^{-3}. Both results from size-selected chemical mixtures and chemical resolution comparison between EESI-TOF and FIGAERO-CI-ToF-MS using a complex SOA mixture indicate that the EESI sensitivity size dependence is a function of the Brownian coagulation coefficient rather than molecular size, polarity, or volatility. Aside from the size dependence, we did not observe any systematic RH influence on the EESI sensitivity from particle size selection (30 - 40 % RH) and SOA formation in the CLOUD chamber (20 - 60% RH) experiments. This is consistent with the findings by Lopez-Hilfiker et al. (2019), where RH does not systematically affect EESI sensitivity, but instead shows molecule-dependent effects where within an internally mixed particle ensemble the sensitivity of certain molecules may increase with RH while others decrease. The enhancement in EESI sensitivity for wet aerosol over dry aerosol was reported in a previous study (Kumbhani et al. 2018). If EESI extraction is limited to the surface of the analyte aerosol, the aerosol water content may mobilize surface species to facilitate dissolution (Kumbhani et al. 2018). However, the lack of RH dependence for our EESI setup indicates that such surface extraction limitation is absent in our study.

3.2 Influence of particles coating thickness on EESI sensitivity

Limited surface extraction, approximately 2-4 nm in depth, of the particles was reported for some ESI source designs (Kumbhani et al., 2018; Wingen and Finlayson-Pitts 2019). If such an effect were present in the EESI-TOF design used in the current study, it could also appear as a size-dependent sensitivity. This would mean that a smaller fraction of the analyte volume is extracted as the particles diameter increases, and that the EESI sensitivity scales with the particle surface area rather than the volume. To determine the potential contribution by surface extraction to the observed sensitivity size dependence, we investigated the extraction efficiency of NH_4NO_3 particles of 156 and 226 nm in diameter before being coated by the α-pinene oxidation products using source A. Source A was chosen because it has the greatest extent of size-dependent sensitivity in comparison to source B. This size range was chosen as the size-dependent sensitivity decreases by less than 15 % from 155 nm to 250 nm for single and mixed component particles (Figure 2). The coating thickness on the NH_4NO_3 particles ranged between 12 and 26 nm, with a coated organic mass concentration up to 31 μg m^{-3} (Figure S11).

If extraction were limited by the particle surface, the EESI signal for NH_4NO_3, i.e. $[NaNO_3+Na]^+$, should decrease similar to the size-dependent sensitivity (Figure 2) that is exhibited by the source A. If the coated particles were of core-shell morphology, then the extraction of the NH_4NO_3 core would be limited by the thickness of the organic coating and the ES extraction depth. If the coated particles were of homogeneous inorganic-organic mixture, then the detected NH_4NO_3 signal would decrease in proportion to the decreasing NH_4NO_3 mass fraction. In Figure 4, we show the signals of NH_4NO_3 and selected organic molecules with low volatility as a function of the coating volume (normalized to their respective minimum coating volume separately for each of the NH_4NO_3 particle core sizes). We find that the coating signal from $C_{10}H_{16}O_{6-8}$ is proportional to the coating volume, whereas the NH_4NO_3 particles signal remains constant with increasing coating thickness for both core sizes (see also Figure S12). This proportionality also demonstrates that the condensable species as coating substance is not limited by the mean oxidation states of oxidation products because there is no decrease of the $C_{10}H_{16}O_6$ for an increase of $C_{10}H_{16}O_8$. Our results suggest that there is no surface extraction limitation for particles up to at least 250 nm in diameter for the EESI inlet designs used in the current study. Prior reporting of surface extraction limitation may stem from the specific EESI configuration or experimental method used, which relied on the comparison of EESI and ESI measurements (Kumbhani et al., 2018), while the differences in dissolution/extraction timescale and sample preparation between EESI and ESI techniques could contribute to the discrepancies observed.

4 Conclusion

We explored the EESI sensitivity response for size-selected particles using individual chemical standards and chemical mixtures with two different EESI source designs. We show that the EESI sensitivity decreases as the size of the particles increases. The sensitivity size dependence correlates with the Brownian coagulation coefficient, where the magnitude of the size-dependent sensitivity can be accounted for by the total particle mass coagulated with the ES droplets according to the residence time for coagulation. This suggests that the particles undergo coalescence with the ES charged droplets as suggested in previous studies (Law et al., 2010; Wang et al., 2012), but the efficiency of the coalescence is limited by the coagulation coefficient related to the different particles and ES charged droplet sizes. From a comparison with online FIGAERO-CI-ToF-MS with measurements we conclude that the EESI sensitivity size dependence still exhibits in an internally mixed secondary organic aerosol made of molecules with volatilities varying by approximately 10 orders of magnitudes. Coating experiments show that the volume of particles is fully extracted up to a size of 250 nm for our EESI configuration but the total extracted mass is limited by the size-dependent Brownian coagulation coefficients (i.e. not all particles of different size can coalesce with all the electrospray droplets) instead of limited surface extraction reported by the previous work (Kumbhani et al., 2018). Future work should investigate the EESI response to coarse mode particles (with $D_p > 1$ μm), elucidate the relationship between size-dependent sensitivity behaviour and different chemical mixtures and search for an optimal residence time for coagulation in the EESI source to achieve the least steep size-dependent sensitivity for the particle size of interest. EESI users should be cognizant of the size-dependent sensitivity during their result interpretation. Such size dependence is especially relevant when studying aerosol formation and growth, and external mixtures of particles with largely different sizes. However, such effect is not expected to substantially influence the detection of ambient aerosols dominated by well-mixed accumulation mode particles.

Data availability. Data presented in this study can be obtained at the Zenodo online repository hosted by CERN (https://doi.org/10.5281/zenodo.4437079, Lee et al., 2021). Raw data can be obtained by contacting the corresponding authors.

Author contributions. C.P.L. and M.S. designed the experiment. M.S., C.P.L., D.W., H.L, M.W., F.A., V. H., B. L., performed the experiments. C.P.L., M.S., M.W., F.A. analyzed the data. C.P.L., I.E., M.S., D.W., H. L., J. D., J.S. and U.B. interpreted the compiled results. C.P.L. prepared the manuscript. All authors contributed to the discussion and revision of the manuscript.

Competing interests. The authors declare that they have no conflict of interest.

Acknowledgements. We thank our technician Pascal Andre Schneider for technical support throughout our experiments and Martin Gysel for the scientific discussion. Special thanks to the CLOUD collaboration and CERN facilities for providing us the possibilities and resources to realize the investigation of the EESI extraction efficiency using complex particles and comparison to other well-known aerosol mass spectrometry techniques.

Financial support. This work was financially supported by the Swiss National Science Foundation (20020_172602, BSSGI0_155846), the European Union's Horizon 2020 research and innovation program under the Marie Skłodowska-Curie actions (No. 701647, No. 764991), US National Science Foundation (AGS1801574, AGS1531284) and EUROCHAMP-2020 projects and infrastructure (No. 730997).

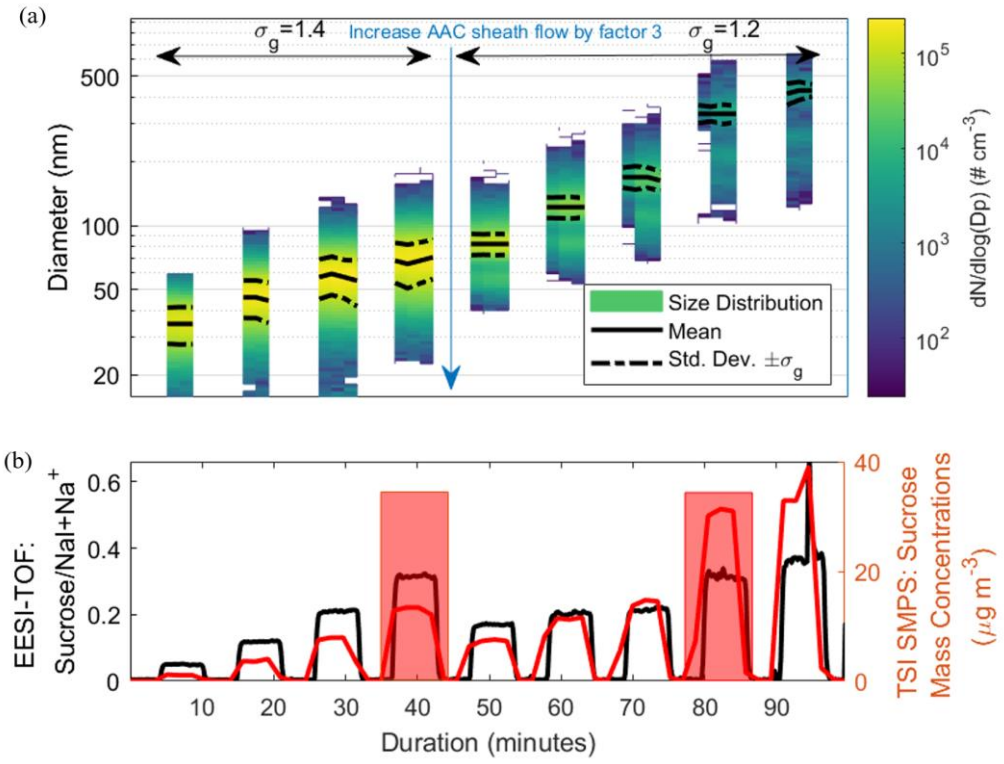

Figure 1. (a) Measured number-weighted size distribution of sucrose particles after size selection using the AAC at two different settings of the AAC sheath flow. The black solid line and the dotted lines denote geometric mean and standard deviation of the number-weighted size distributions, respectively. σ_g is the geometric standard deviation of the number-weighted size distribution. The full width at half maximum (FWHM) of the size-selected particle distribution of sucrose is lower at the higher sheath flow of the AAC. Data points of particle counts lower than 1 cm^{-3} were removed. Please see Figure S5 for the size-selection performance of the AAC. (b) A representative EESI-TOF measurement that shows the time series of sucrose normalized to the NaI+Na$^+$ signal (ES ion) and the corresponding integrated particle mass concentration measured by the TSI SMPS for size-selected sucrose particles (using the integrated volume concentration and a density of 1.59 g cm^{-3}). Red windows indicate periods with the same EESI signal of sucrose but different size and mass concentration.

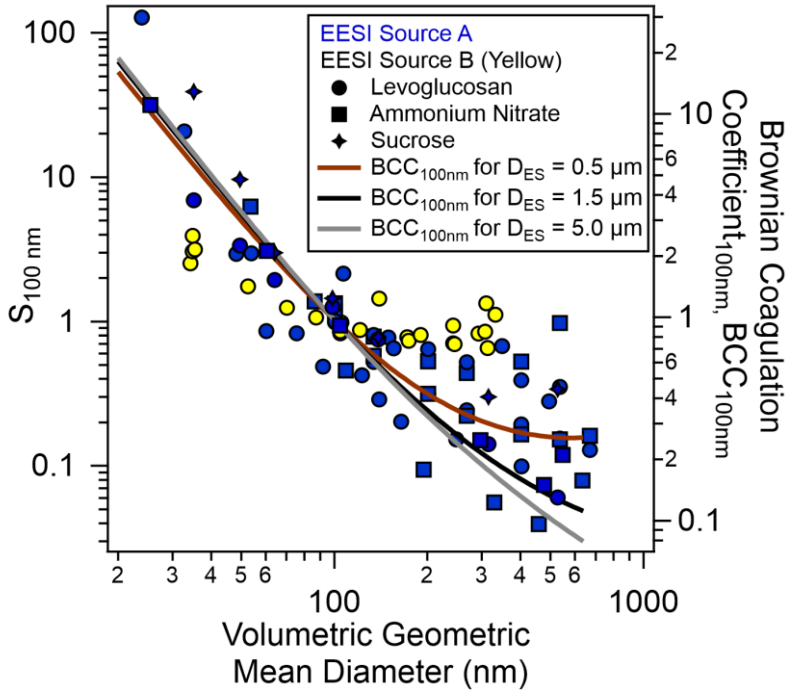

Figure 2. Sensitivity of EESI-TOF measurements normalized at 100 nm as a function of volumetric geometric mean diameter. Blue and yellow markers indicate EESI source A and B which were initially developed for TOF and Orbitrap mass analyzers, respectively (Lopez-Hilfiker et al., 2019; Lee et al., 2020). Different marker types (●), (■), (✦) denote levoglucosan, NH_4NO_3 and sucrose, respectively. The Brownian coagulation coefficients are calculated using the range of ES parent droplet sizes estimated according to our ES operating parameters (Figures S6 and S7). Note: Some of the data points may overlap at the similar volumetric geometric mean diameter due to repetitions of the same experiment settings.

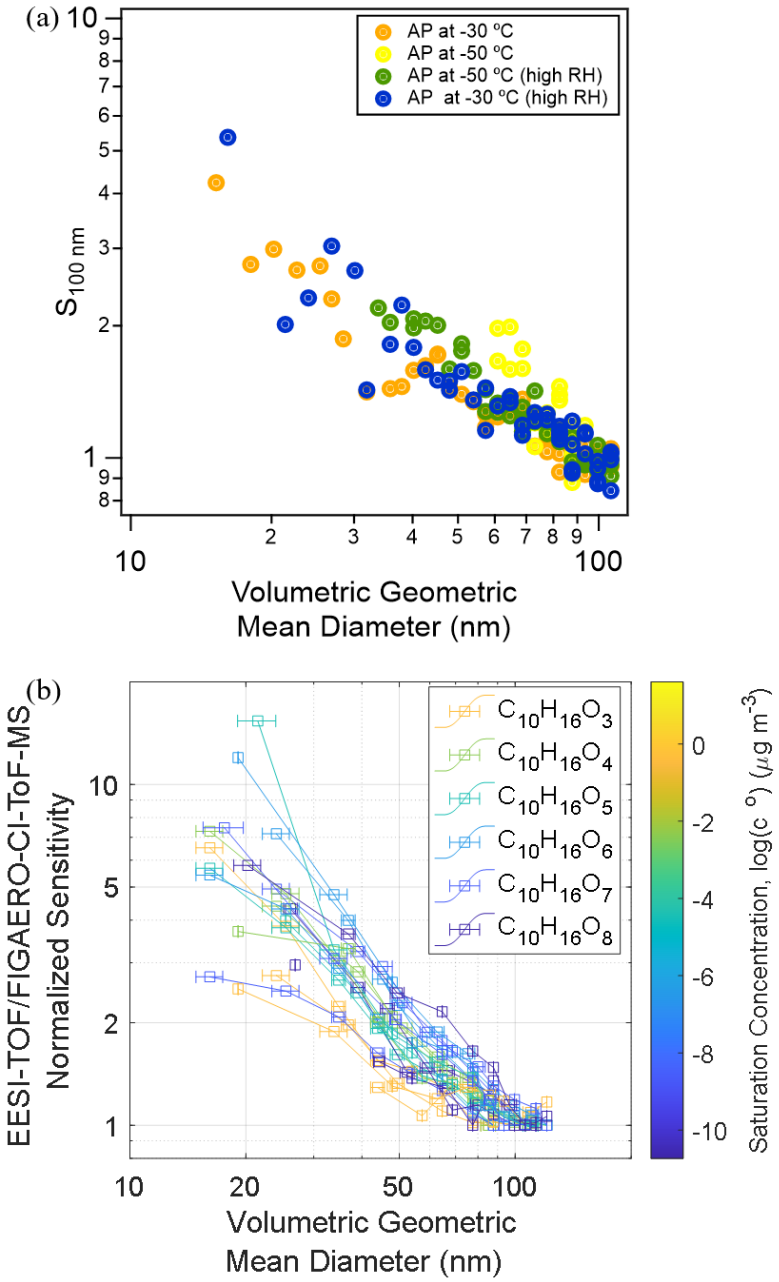

Figure 3. (a) Normalized sensitivity of EESI-TOF sum of high-resolution fitted organic ions as a function of the volume-weighted geometric mean diameter for each particle growth event in the α-pinene (AP) system at -30 and -50 ˚C. (b) Normalized sensitivity of EESI-TOF intensity divided by the FIGAERO-CI-ToF-MS intensity for $C_{10}H_{16}O_{3\text{-}8}$ molecules in the particle phase as a function of the volume-weighted geometric mean diameter. Different marker types □, ∗, ○, + indicate different SOA formation runs at -30 ˚C, -50 ˚C, -50 ˚C (high RH) and -30 ˚C (high RH), respectively. The saturation concentration was estimated as $log_{10}(C^0) = (n_C^0 - n_C)b_c - n_O b_O - 2 \cdot b_{CO}(n_C n_O)/(n_C + n_O)$ using the number of carbon and oxygen (n_C, n_O), interaction terms of carbon-carbon, oxygen-oxygen and carbon-oxygen (b_c, b_O, b_{CO}) and carbon number of alkane with a saturation vapor pressure of 1 μg m^{-3} ($n_C^0 = 25$) at 300 K (Donahue et al., 2011). See Figures S8, S9 and S10 for more information.

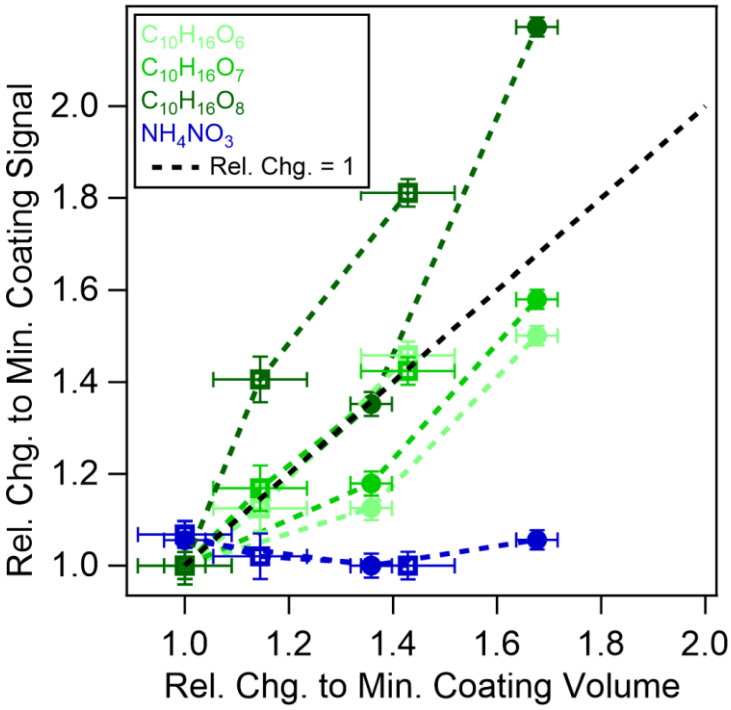

Figure 4. Relative changes of α-pinene ozonolysis products coated on NH_4NO_3 particles at 156 (●) and 226 (■) nm core sizes. The coating volume (*x*-axis) measured by an SMPS is normalized by the smallest coating volume, and the coating signals (*y*-axis) of $C_{10}H_{16}O_{6\text{-}8}$ molecules as measured by the EESI-TOF are normalized by the signal at the smallest coating volume. The largest coating thicknesses are 19.8 and 26.8 nm for 156 and 226 nm core sizes of the NH_4NO_3 particles. The black-dotted line denotes a relative change of the coating signal and volume equal to 1.

References

Berndt, T., Böge, O., Stratmann, F., Heintzenberg, J. and Kulmala, M.: Rapid formation of sulfuric acid particles at near-atmospheric conditions, Science, 307(5710), 698–700, doi:10.1126/science.1104054, 2005.

Burnett, R., Chen, H., Szyszkowicz, M., Fann, N., Hubbell, B., Pope, C. A., Apte, J. S., Brauer, M., Cohen, A., Weichenthal, S., Coggins, J., Di, Q., Brunekreef, B., Frostad, J., Lim, S. S., Kan, H., Walker, K. D., Thurston, G. D., Hayes, R. B., Lim, C. C., Turner, M. C., Jerrett, M., Krewski, D., Gapstur, S. M., Diver, W. R., Ostro, B., Goldberg, D., Crouse, D. L., Martin, R. V., Peters, P., Pinault, L., Tjepkema, M., Van Donkelaar, A., Villeneuve, P. J., Miller, A. B., Yin, P., Zhou, M., Wang, L., Janssen, N. A. H., Marra, M., Atkinson, R. W., Tsang, H., Thach, T. Q., Cannon, J. B., Allen, R. T., Hart, J. E., Laden, F., Cesaroni, G., Forastiere, F., Weinmayr, G., Jaensch, A., Nagel, G., Concin, H. and Spadaro, J. V.: Global estimates of mortality associated with longterm exposure to outdoor fine particulate matter, Proc. Natl. Acad. Sci. U. S. A., 115(38), 9592–9597, doi:10.1073/pnas.1803222115, 2018.

Chen, H., Venter, A. and Cooks, R. G.: Extractive electrospray ionization for direct analysis of undiluted urine, milk and other complex mixtures without sample preparation, Chem. Commun., 0(19), 2042–2044, doi:10.1039/b602614a, 2006.

Cheng, C. Y., Yuan, C. H., Cheng, S. C., Huang, M. Z., Chang, H. C., Cheng, T. L., Yeh, C. S. and Shiea, J.: Electrospray-assisted laser desorption/ionization mass spectrometry for continuously monitoring the states of ongoing chemical reactions in organic or aqueous solution under ambient conditions, Anal. Chem., 80(20), 7699–7705, doi:10.1021/ac800952e, 2008.

Clarke, A. G., Willison, M. J. and Zeki, E. M.: Aerosol Neutralization by Atmospheric Ammonia, in Physico-Chemical Behaviour of Atmospheric Pollutants, pp. 331–338, Springer Netherlands., 1984.

Daellenbach, K.: Sources of particulate matter air pollution and its oxidative potential in Europe, Nature, doi:10.1038/s41586-020-2902-8, 2020.

Dias, A., Ehrhart, S., Vogel, A., Williamson, C., Almeida, J., Kirkby, J., Mathot, S., Mumford, S. and Onnela, A.: Temperature uniformity in the CERN CLOUD chamber, Atmos. Meas. Tech., 10(12), 5075–5088, doi:10.5194/amt-10-5075-2017, 2017.

Ditto, J. C., Joo, T., Slade, J. H., Shepson, P. B., Ng, N. L. and Gentner, D. R.: Nontargeted Tandem Mass Spectrometry Analysis Reveals Diversity and Variability in Aerosol Functional Groups across Multiple Sites, Seasons, and Times of Day, Environ. Sci. Technol. Lett., 7(2), 60–69, doi:10.1021/acs.estlett.9b00702, 2020.

Donahue, N. M., Epstein, S. A., Pandis, S. N. and Robinson, A. L.: A two-dimensional volatility basis set: 1. organic-aerosol mixing thermodynamics, Atmos. Chem. Phys., 11(7), 3303–3318, doi:10.5194/acp-11-3303-2011, 2011.

Eichler, P., Müller, M., D'Anna, B. and Wisthaler, A.: A novel inlet system for online chemical analysis of semi-volatile submicron particulate matter, Atmos. Meas. Tech., 8(3), 1353–1360, doi:10.5194/amt-8-1353-2015, 2015.

George, I. J. and Abbatt, J. P. D.: Heterogeneous oxidation of atmospheric aerosol particles by gas-phase radicals, Nat. Chem., 2(9), 713–722, doi:10.1038/nchem.806, 2010.

Giannoukos, S., Lee, C. P., Tarik, M., Ludwig, C., Biollaz, S., Lamkaddam, H., Baltensperger, U., Henry Prevot, A. S. and Slowik, J.: Real-Time Detection of Aerosol Metals Using Online Extractive Electrospray Ionization Mass Spectrometry, Anal. Chem., 92(1), 1316–1325, doi:10.1021/acs.analchem.9b04480, 2020.

Hoffmann, T., Odum, J. R., Bowman, F., Collins, D., Klockow, D., Flagan, R. C. and Seinfeld, J. H.: Formation of organic aerosols from the oxidation of biogenic hydrocarbons, J. Atmos. Chem., 26(2), 189–222, doi:10.1023/A:1005734301837, 1997.

Holzinger, R., Williams, J., Herrmann, F., Lelieveld, J., Donahue, N. M. and Röckmann, T.: Aerosol analysis using a Thermal-Desorption Proton-Transfer-Reaction Mass Spectrometer (TD-PTR-MS): A new approach to study processing of organic aerosols., 2010.

Jimenez, J. L., Canagaratna, M. R., Donahue, N. M., Prevot, A. S. H., Zhang, Q., Kroll, J. H., DeCarlo, P. F., Allan, J. D., Coe, H., Ng, N. L., Aiken, A. C., Docherty, K. S., Ulbrich, I. M., Grieshop, A. P., Robinson, A. L., Duplissy, J., Smith, J. D., Wilson, K. R., Lanz, V. A., Hueglin, C., Sun, Y. L., Tian, J., Laaksonen, A., Raatikainen, T., Rautiainen, J., Vaattovaara, P., Ehn, M., Kulmala, M., Tomlinson, J. M., Collins, D. R., Cubison, M. J., Dunlea, E. J., Huffman, J. A., Onasch, T. B., Alfarra, M. R., Williams, P. I., Bower, K., Kondo, Y., Schneider, J., Drewnick, F., Borrmann, S., Weimer, S., Demerjian, K., Salcedo,

D., Cottrell, L., Griffin, R., Takami, A., Miyoshi, T., Hatakeyama, S., Shimono, A., Sun, J. Y., Zhang, Y. M., Dzepina, K., Kimmel, J. R., Sueper, D., Jayne, J. T., Herndon, S. C., Trimborn, A. M., Williams, L. R., Wood, E. C., Middlebrook, A. M., Kolb, C. E., Baltensperger, U. and Worsnop, D. R.: Evolution of organic aerosols in the atmosphere, Science, 326(5959), 1525–1529, doi:10.1126/science.1180353, 2009.

Kalberer, M., Paulsen, D., Sax, M., Steinbacher, M., Dommen, J., Prevot, A. S. H., Fisseha, R., Weingartner, E., Frankevich, V., Zenobi, R. and Baltensperger, U.: Identification of Polymers as Major Components of Atmospheric Organic Aerosols, Science, 303(5664), 1659–1662, doi:10.1126/science.1092185, 2004.

Kebarle, P. and Verkcerk, U. H.: Electrospray: From Ions in solution to Ions in the gas phase, what we know now, Mass Spectrom. Rev., 28(6), 898–917, doi:10.1002/mas.20247, 2009.

Kebarle, P. and Verkerk, U. H.: On the Mechanism of Electrospray Ionization Mass Spectrometry (ESIMS), Electrospray MALDI Mass Spectrom. Fundam. Instrumentation, Pract. Biol. Appl. Second Ed., 82(11), 1–48, doi:10.1002/9780470588901.ch1, 2012.

Kirkby, J., Curtius, J., Almeida, J., Dunne, E., Duplissy, J., Ehrhart, S., Franchin, A., Gagné, S., Ickes, L., Kürten, A., Kupc, A., Metzger, A., Riccobono, F., Rondo, L., Schobesberger, S., Tsagkogeorgas, G., Wimmer, D., Amorim, A., Bianchi, F., Breitenlechner, M., David, A., Dommen, J., Downard, A., Ehn, M., Flagan, R. C., Haider, S., Hansel, A., Hauser, D., Jud, W., Junninen, H., Kreissl, F., Kvashin, A., Laaksonen, A., Lehtipalo, K., Lima, J., Lovejoy, E. R., Makhmutov, V., Mathot, S., Mikkilä, J., Minginette, P., Mogo, S., Nieminen, T., Onnela, A., Pereira, P., Petäjä, T., Schnitzhofer, R., Seinfeld, J. H., Sipilä, M., Stozhkov, Y., Stratmann, F., Tomé, A., Vanhanen, J., Viisanen, Y., Vrtala, A., Wagner, P. E., Walther, H., Weingartner, E., Wex, H., Winkler, P. M., Carslaw, K. S., Worsnop, D. R., Baltensperger, U. and Kulmala, M.: Role of sulphuric acid, ammonia and galactic cosmic rays in atmospheric aerosol nucleation, Nature, 476(7361), 429–435, doi:10.1038/nature10343, 2011.

Kirkby, J., Duplissy, J., Sengupta, K., Frege, C., Gordon, H., Williamson, C., Heinritzi, M., Simon, M., Yan, C., Almeida, J., Trostl, J., Nieminen, T., Ortega, I. K., Wagner, R., Adamov, A., Amorim, A., Bernhammer, A. K., Bianchi, F., Breitenlechner, M., Brilke, S., Chen, X., Craven, J., Dias, A., Ehrhart, S., Flagan, R. C., Franchin, A., Fuchs, C., Guida, R., Hakala, J., Hoyle, C. R., Jokinen, T., Junninen, H., Kangasluoma, J., Kim, J., Krapf, M., Kurten, A., Laaksonen, A., Lehtipalo, K., Makhmutov, V., Mathot, S., Molteni, U., Onnela, A., Perakyla, O., Piel, F., Petaja, T., Praplan, A. P., Pringle, K., Rap, A., Richards, N. A. D., Riipinen, I., Rissanen, M. P., Rondo, L., Sarnela, N., Schobesberger, S., Scott, C. E., Seinfeld, J. H., Sipila, M., Steiner, G., Stozhkov, Y., Stratmann, F., Tomé, A., Virtanen, A., Vogel, A. L., Wagner, A. C., Wagner, P. E., Weingartner, E., Wimmer, D., Winkler, P. M., Ye, P., Zhang, X., Hansel, A., Dommen, J., Donahue, N. M., Worsnop, D. R., Baltensperger, U., Kulmala, M., Carslaw, K. S. and Curtius, J.: Ion-induced nucleation of pure biogenic particles, Nature, 533(7604), 521–526, doi:10.1038/nature17953, 2016.

Konermann, L., Ahadi, E., Rodriguez, A. D. and Vahidi, S.: Unraveling the mechanism of electrospray ionization, Anal. Chem., 85(1), 2–9, doi:10.1021/ac302789c, 2013.

Kumbhani, S., Longin, T., Wingen, L. M., Kidd, C., Perraud, V. and Finlayson-Pitts, B. J.: New Mechanism of Extractive Electrospray Ionization Mass Spectrometry for Heterogeneous Solid Particles, Anal. Chem., 90(3), 2055–2062, doi:10.1021/acs.analchem.7b04164, 2018.

Law, W. S., Wang, R., Hu, B., Berchtold, C., Meier, L., Chen, H. and Zenobi, R.: On the mechanism of extractive electrospray ionization, Anal. Chem., 82(11), 4494–4500, doi:10.1021/ac100390t, 2010.

Lee, C. P., Riva, M., Wang, D., Tomaz, S., Li, D., Perrier, S., Slowik, J. G., Bourgain, F., Schmale, J., Prevot, A. S. H., Baltensperger, U., George, C. and El Haddad, I.: Online Aerosol Chemical Characterization by Extractive Electrospray Ionization-Ultrahigh-Resolution Mass Spectrometry (EESI-Orbitrap), Environ. Sci. Technol., 54(7), 3871–3880, doi:10.1021/acs.est.9b07090, 2020.

Lopez-Hilfiker, F. D., Mohr, C., Ehn, M., Rubach, F., Kleist, E., Wildt, J., Mentel, T. F., Lutz, A., Hallquist, M., Worsnop, D. and Thornton, J. A.: A novel method for online analysis of gas and particle composition: Description and evaluation of a filter inlet for gases and AEROsols (FIGAERO), Atmos. Meas. Tech., 7(4), 983–1001, doi:10.5194/amt-7-983-2014, 2014.

Lopez-Hilfiker, F. D., Pospisilova, V., Huang, W., Kalberer, M., Mohr, C., Stefenelli, G., Thornton, J. A., Baltensperger, U., Prevot, A. S. H. and Slowik, J. G.: An extractive electrospray ionization time-of-flight mass spectrometer (EESI-TOF) for online measurement of atmospheric aerosol particles, Atmos. Meas. Tech., 12(9), 4867–4886, doi:10.5194/amt-12-4867-2019,

2019.

Marquez, C. A., Wang, H., Fabbretti, F. and Metzger, J. O.: Electron-transfer-catalyzed dimerization of trans-anethole: Detection of the distonic tetramethylene radical cation intermediate by extractive electrospray ionization mass spectrometry, J. Am. Chem. Soc., 130(51), 17208–17209, doi:10.1021/ja806791c, 2008.

Meier, L., Schmid, S., Berchtold, C. and Zenobi, R.: Contribution of liquid-phase and gas-phase ionization in extractive electrospray ionization mass spectrometry of primary amines, Eur. J. Mass Spectrom., 17(4), 345–351, doi:10.1255/ejms.1146, 2011a.

Meier, L., Schmid, S., Berchtold, C. and Zenobi, R.: Contribution of liquid-phase and gas-phase ionization in extractive electrospray ionization mass spectrometry of primary amines, Eur. J. Mass Spectrom., 17(4), 345–351, doi:10.1255/ejms.1146, 2011b.

Molteni, U., Bianchi, F., Klein, F., El Haddad, I., Frege, C., Rossi, M. J., Dommen, J. and Baltensperger, U.: Formation of highly oxygenated organic molecules from aromatic compounds, Atmos. Chem. Phys., 18(3), 1909–1921, doi:10.5194/acp-18-1909-2018, 2018.

Müller, M., Eichler, P., D'Anna, B., Tan, W. and Wisthaler, A.: Direct Sampling and Analysis of Atmospheric Particulate Organic Matter by Proton-Transfer-Reaction Mass Spectrometry, Anal. Chem., 89(20), 10889–10897, doi:10.1021/acs.analchem.7b02582, 2017.

Pagonis, D.: Airborne Extractive Electrospray Mass Spectrometry Measurements of the Chemical Composition of Organic Aerosol, Submitt. To Atmos. Meas. Tech., in review, doi:10.5194/amt-2020-395, 2020.

Simon, M., Dada, L., Heinritzi, M., Scholz, W., Stolzenburg, D., Fischer, L., Wagner, A., Kürten, A., Rörup, B., He, X.-C., Almeida, J., Baalbaki, R., Baccarini, A., Bauer, P., Beck, L., Bergen, A., Bianchi, F., Bräkling, S., Brilke, S., Caudillo, L., Chen, D., Chu, B., Dias, A., Draper, D., Duplissy, J., El Haddad, I., Finkenzeller, H., Frege, C., Gonzalez-Carracedo, L., Gordon, H., Granzin, M., Hakala, J., Hofbauer, V., Hoyle, C., Kim, C., Kong, W., Lamkaddam, H., Lee, C., Lehtipalo, K., Leiminger, M., Mai, H., Manninen, H., Marie, G., Marten, R., Mentler, B., Molteni, U., Nichman, L., Nie, W., Ojdanic, A., Onnela, A., Partoll, E., Petäjä, T., Pfeifer, J., Philippov, M., Quéléver, L., Ranjithkumar, A., Rissanen, M., Schallhart, S., Schobesberger, S., Schuchmann, S., Shen, J., Sipilä, M., Steiner, G., Stozhkov, Y., Tauber, C., Tham, Y., Tomé, A., Vazquez-Pufleau, M., Vogel, A., Wagner, R., Wang, M., Wang, D., Wang, Y., Weber, S., Wu, Y., Xiao, M., Yan, C., Ye, P., Ye, Q., Zauner-Wieczorek, M., Zhou, X., Baltensperger, U., Dommen, J., Flagan, R., Hansel, A., Kulmala, M., Volkamer, R., Winkler, P., Worsnop, D., Donahue, N., Kirkby, J. and Curtius, J.: Molecular understanding of new-particle formation from alpha-pinene between −50 °C and 25 °C, Atmos. Chem. Phys., 40(January), 1–42, doi:10.5194/acp-2019-1058, 2020.

Stark, H., Yatavelli, R. L. N., Thompson, S. L., Kang, H., Krechmer, J. E., Kimmel, J. R., Palm, B. B., Hu, W., Hayes, P. L., Day, D. A., Campuzano-Jost, P., Canagaratna, M. R., Jayne, J. T., Worsnop, D. R. and Jimenez, J. L.: Impact of Thermal Decomposition on Thermal Desorption Instruments: Advantage of Thermogram Analysis for Quantifying Volatility Distributions of Organic Species, Environ. Sci. Technol., 51(15), 8491–8500, doi:10.1021/acs.est.7b00160, 2017.

Steinfeld, J. I.: Atmospheric Chemistry and Physics: From Air Pollution to Climate Change, 3rd ed., Wiley Publication., 1998.

Tavakoli, F. and Olfert, J. S.: An instrument for the classification of aerosols by particle relaxation time: Theoretical models of the aerodynamic aerosol classifier, Aerosol Sci. Technol., 47(8), 916–926, doi:10.1080/02786826.2013.802761, 2013.

Tavakoli, F. and Olfert, J. S.: Determination of particle mass, effective density, mass-mobility exponent, and dynamic shape factor using an aerodynamic aerosol classifier and a differential mobility analyzer in tandem, J. Aerosol Sci., 75, 35–42, doi:10.1016/j.jaerosci.2014.04.010, 2014.

Tavakoli, F., Symonds, J. P. R. and Olfert, J. S.: Generation of a monodisperse size-classified aerosol independent of particle charge, Aerosol Sci. Technol., 48(3), i–iv, doi:10.1080/02786826.2013.877121, 2014.

Tröstl, J., Chuang, W. K., Gordon, H., Heinritzi, M., Yan, C., Molteni, U., Ahlm, L., Frege, C., Bianchi, F., Wagner, R., Simon, M., Lehtipalo, K., Williamson, C., Craven, J. S., Duplissy, J., Adamov, A., Almeida, J., Bernhammer, A. K., Breitenlechner, M., Brilke, S., Dias, A., Ehrhart, S., Flagan, R. C., Franchin, A., Fuchs, C., Guida, R., Gysel, M., Hansel, A., Hoyle, C. R., Jokinen, T., Junninen, H., Kangasluoma, J., Keskinen, H., Kim, J., Krapf, M., Kürten, A., Laaksonen, A., Lawler, M., Leiminger, M., Mathot, S., Möhler, O., Nieminen, T., Onnela, A., Petäjä, T., Piel, F. M., Miettinen, P., Rissanen, M. P., Rondo, L., Sarnela, N., Schobesberger, S., Sengupta, K., Sipilä, M., Smith, J. N., Steiner, G., Tomè, A., Virtanen, A., Wagner, A. C.,

Weingartner, E., Wimmer, D., Winkler, P. M., Ye, P., Carslaw, K. S., Curtius, J., Dommen, J., Kirkby, J., Kulmala, M., Riipinen, I., Worsnop, D. R., Donahue, N. M. and Baltensperger, U.: The role of low-volatility organic compounds in initial particle growth in the atmosphere, Nature, 533(7604), 527–531, doi:10.1038/nature18271, 2016.

Wagner, A. C., Bergen, A., Brilke, S., Fuchs, C., Ernst, M., Hoker, J., Heinritzi, M., Simon, M., Bühner, B., Curtius, J. and Kürten, A.: Size-resolved online chemical analysis of nanoaerosol particles: A thermal desorption differential mobility analyzer coupled to a chemical ionization time-of-flight mass spectrometer, Atmos. Meas. Tech., 11(10), 5489–5506, doi:10.5194/amt-11-5489-2018, 2018.

Wang, R., Gröhn, A. J., Zhu, L., Dietiker, R., Wegner, K., Günther, D. and Zenobi, R.: On the mechanism of extractive electrospray ionization (EESI) in the dual-spray configuration, Anal. Bioanal. Chem., 402(8), 2633–2643, doi:10.1007/s00216-011-5471-8, 2012.

Wingen, L. M. and Finlayson-Pitts, B. J.: Probing surfaces of atmospherically relevant organic particles by easy ambient sonic-spray ionization mass spectrometry (EASI-MS), Chem. Sci., 10(3), 884–897, doi:10.1039/c8sc03851a, 2019.

Yue, D., Hu, M., Wu, Z., Wang, Z., Guo, S., Wehner, B., Nowak, A., Achtert, P., Wiedensohler, A., Jung, J., Kim, Y. J. and Liu, S.: Characteristics of aerosol size distributions and new particle formation in the summer in Beijing, J. Geophys. Res. Atmos., 114(14), doi:10.1029/2008JD010894, 2009.